nature genetics

Mutations in *WDR62*, encoding a centrosome-associated protein, cause microcephaly with simplified gyri and abnormal cortical architecture

Timothy W Yu[1–7], Ganeshwaran H Mochida[1–7], David J Tischfield[1–5], Sema K Sgaier[1–5,8], Laura Flores-Sarnat[9], Consolato M Sergi[10,11], Meral Topçu[12], Marie T McDonald[13], Brenda J Barry[1–5], Jillian M Felie[1–5], Christine Sunu[1–5], William B Dobyns[14], Rebecca D Folkerth[15], A James Barkovich[16] & Christopher A Walsh[1–6]

Genes associated with human microcephaly, a condition characterized by a small brain, include critical regulators of proliferation, cell fate and DNA repair. We describe a syndrome of congenital microcephaly and diverse defects in cerebral cortical architecture. Genome-wide linkage analysis in two families identified a 7.5-Mb locus on chromosome 19q13.12 containing 148 genes. Targeted high throughput sequence analysis of linked genes in each family yielded > 4,000 DNA variants and implicated a single gene, *WDR62*, as harboring potentially deleterious changes. We subsequently identified additional *WDR62* mutations in four other families. Magnetic resonance imaging and postmortem brain analysis supports important roles for *WDR62* in the proliferation and migration of neuronal precursors. WDR62 is a WD40 repeat–containing protein expressed in neuronal precursors as well as in postmitotic neurons in the developing brain and localizes to the spindle poles of dividing cells. The diverse phenotypes of WDR62 suggest it has central roles in many aspects of cerebral cortical development.

A first pedigree (LIS-900) with microcephaly with simplified gyri (MCSG) from Mexico consisted of distantly related parents with three affected children and one healthy child (**Fig. 1a**). The children showed severe microcephaly, developmental delay and seizures (**Supplementary Note**) but no other syndromic features. A second family (LIS-2600) from Turkey showed similar clinical features and has been described before[1] (**Fig. 1b**). Subsequent to the identification of the responsible gene, four other families were identified with similar clinical features (**Fig. 1c–f** and **Supplementary Note**). Brain magnetic resonance imaging (MRI) of the six families (**Fig. 1g–p**) revealed small brains, markedly simplified gyral patterns and corpus callosal abnormalities, as well as a diversity of additional cortical malformations including polymicrogyria, schizencephaly and subcortical heterotopia (arrested neurons), sometimes with asymmetry in the same brain (**Supplementary Note** and **Supplementary Movie 1**).

Homozygosity mapping in LIS-900 showed a single 11.9-Mb region on chromosome 19q13 (D19S431; D19S217) homozygous in all three affected individuals and not homozygous in the unaffected sibling (**Supplementary Fig. 1**). SNP genotyping of LIS-2600 confirmed the homozygosity and narrowed the interval to approximately 7.5 Mb (**Fig. 2a**) (peak combined multipoint $\log_{10}$ odds (LOD) score of 3.84; **Supplementary Fig. 2**). SNP analysis of MC-1400 and MC-1600 confirmed the candidate region but did not reduce it (**Fig. 2a**).

Because of the high gene density of the linked region, we employed an array capture approach[2] followed by high-throughput Illumina sequencing in two affected individuals, LIS-903 and LIS-2602. A custom array was designed with oligonucleotide probes targeting the exons of all 148 predicted UCSC genes in the interval (**Fig. 2b**) plus non-exonic DNA from a smaller candidate subregion suggested by microsatellite mapping (**Supplementary Fig. 2**). DNA bound to the array was amplified and used to generate sequencing libraries. Thirty-six to forty million paired-end sequence tags (>1.4 Gb of

[1]Division of Genetics, Department of Medicine, Children's Hospital Boston, Boston, Massachusetts, USA. [2]Manton Center for Orphan Disease Research, Children's Hospital Boston, Boston, Massachusetts, USA. [3]Howard Hughes Medical Institute, Children's Hospital Boston, Boston, Massachusetts, USA. [4]Department of Pediatrics, Harvard Medical School, Boston, Massachusetts, USA. [5]Department of Neurology, Harvard Medical School, Boston, Massachusetts, USA. [6]Broad Institute of Massachusetts Institute of Technology and Harvard University, Cambridge, Massachusetts, USA. [7]Division of Child Neurology, Department of Neurology, Massachusetts General Hospital, Harvard Medical School, Boston, Massachusetts, USA. [8]Bill and Melinda Gates Foundation, New Delhi, India. [9]Department of Clinical Neurosciences, Division of Paediatric Neurology, Alberta Children's Hospital, University of Calgary Faculty of Medicine, Calgary, Alberta, Canada. [10]Department of Laboratory Medicine and Pathology, University of Alberta Hospital, Walter Mackenzie Health Sciences Centre, Edmonton, Alberta, Canada. [11]Institute of Pathology, Medical University of Innsbruck, Innsbruck, Austria. [12]Department of Pediatrics Section of Pediatric Neurology, Hacettepe University, Medical Faculty, Ihsan Dogramaci Children's Hospital, Ankara, Turkey. [13]Division of Medical Genetics, Department of Pediatrics, Duke University, Durham, North Carolina, USA. [14]Division of Genetics, University of Washington at Seattle, Seattle, Washington, USA. [15]Division of Neuropathology, Brigham and Women's Hospital, Boston, Massachusetts, USA. [16]Department of Radiology, University of California San Francisco, San Francisco, California, USA. Correspondence should be addressed to C.A.W. (christopher.walsh@childrens.harvard.edu).

Received 27 May; accepted 10 September; published online 3 October 2010; doi:10.1038/ng.683

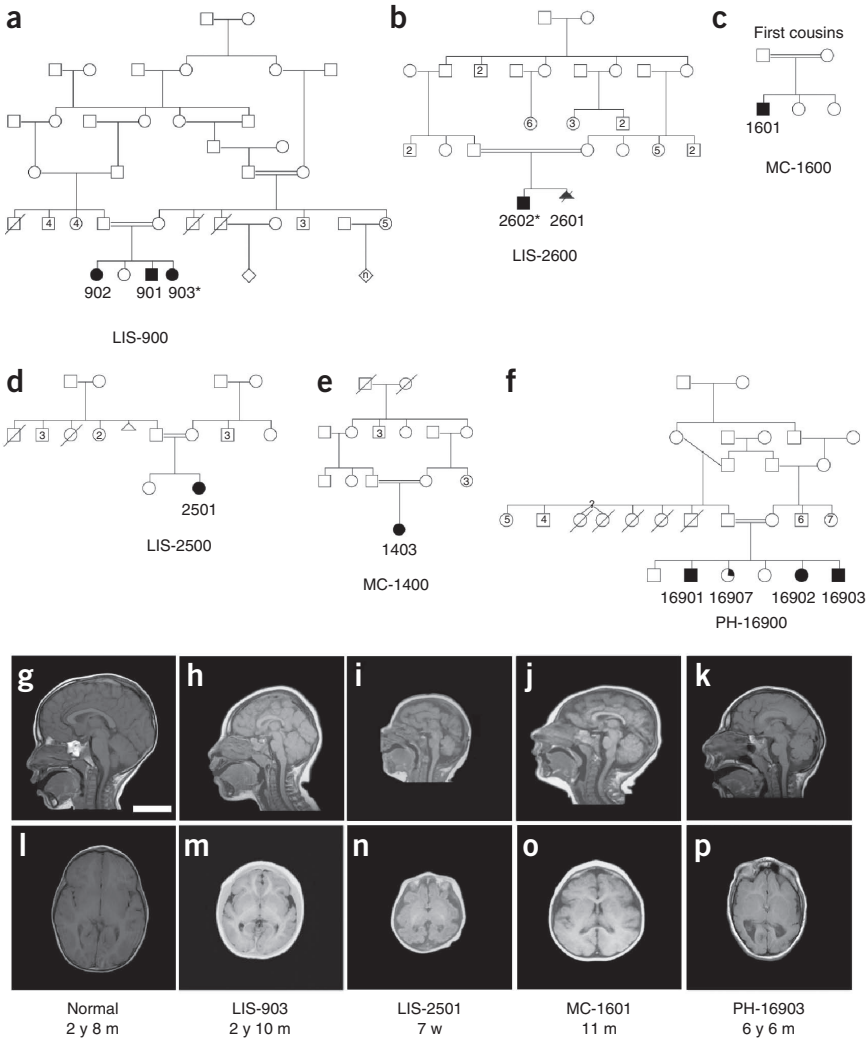

Figure 1 Pedigrees and radiographic findings in six consanguineous families with MCSG. (**a**–**f**) Shaded symbols denote affected individuals. (**a**) LIS-900, a Mexican family with three affected children. (**b**) LIS-2600, a Turkish family with two affected children[1]. (**c**) LIS-2500, (**d**) MC-1400 and (**e**) MC-1600, three Turkish families (not known to be related to LIS-2600 or to each other). (**f**) PH-16900, a Saudi family with three affected children; a fourth child (partial shading) had mild speech delay and articulation and attention difficulties but no brain abnormalities. Whole blood DNA was obtained and analyzed from each nuclear family, with the exception of LIS-2601, who died as a fetus. Asterisks denote the two individuals chosen for targeted high-throughput sequencing. (**g**–**p**) MRI features of individuals with MCSG, demonstrating the breadth of cortical phenotypes associated with *WDR62*. Mid-sagittal T1 sections (**g**–**k**) and axial T1 sections at the level of the insula (**l**–**p**) are shown for LIS-903 (**h**,**m**), LIS-2501 (**i**,**n**), MC-1601 (**j**,**o**) and PH-16903 (**k**,**p**) individuals, as well as a control individual (**g**,**l**) age matched to LIS-903. Common findings include microcephaly (**h**–**k**,**m**–**p**), anomalies of the corpus callosum (small splenium in **h** and **k**, absent splenium in **i** and thick body in **k**), simplification of the normal gyral pattern (**h**,**i**,**k**,**m**,**n**,**p**), as well as more variable features such as mild asymmetries of cortical size (**p**), possible heterotopia and cortical clefts (data not shown; **Supplementary Note**). Scale bar, 5 cm.

raw sequence) were generated per affected individual and mapped (hg18) using the Burrows-Wheeler Alignment tool (BWA) (**Fig. 2c** and ref. 3). Fifty to sixty percent of sequence reads were on target, and the average depth of target coverage was ×230 and ×224, with 88% and 90% of bases covered by ≥10 reads.

Single nucleotide variants, microinsertions and microdeletions were called and filtered for quality and mapping confidence[4], revealing >2,000 potential sequence variants from each proband (**Table 1**). Comparison of SNP calls with Affymetrix 5.0 genotype data showed >99.8% concordance. Variants were filtered out if they were present in dbSNP130 (ref. 4) or the 1000 Genomes Project (see URLs) and categorized by their predicted functional effects using the Genomic Mutation Consequence Calculator (GMCC). Of 2,310 variants in LIS-903, 262 (11%) were not in dbSNP130 or the 1000 Genomes Project, 93 were potentially pathogenic (4.0%) and 5 met both criteria. Of 2,570 variants in LIS-2602, 323 (12%) were absent from dbSNP and the 1000 Genomes Project, 99 (3.8%) were potentially pathogenic and 7 variants met both criteria. A single gene, *WDR62*, showed new, pathogenic mutations in both families, making it a strong candidate (**Table 1**).

Sanger sequencing confirmed *WDR62* mutations in the two families and identified four additional alleles in four other families (**Fig. 3a**,**b** and **Supplementary Fig. 3**). A homozygous single-basepair insertion in exon 30 (c.3936_3937insC) in LIS-2602 produced a frameshift mutation (**Fig. 3b**). All three affected individuals in family LIS-900 showed a homozygous single-basepair deletion in exon 4 (c.363delT), creating a frameshift mutation (**Fig. 3b**). Pedigree analysis confirmed appropriate segregation of *WDR62* mutations in both families (**Fig. 3b**). In LIS-2500, the affected individual showed a homozygous mutation one basepair downstream of exon 8 (c.1043+1G>A) disrupting the highly conserved GT consensus splicing sequence (**Fig. 3a** and **Supplementary Fig. 3**). In MC-1400, the affected child was homozygous for a 4-bp deletion after exon 23 (c.2867+4_c2867+7delGGTG) (**Fig. 3a** and **Supplementary Fig. 3**) that removes the conserved +4 and +5 positions of the intron and is predicted to disrupt the splice donor[5] (reference …CAG|gtgggtgtc…; mutation …CAG|gtg—tc…). In MC-1600, the affected child was homozygous for a 17-bp deletion in the thirtieth exon (c.3839_3855delGCCAAGAGCCTGCCCTG), causing a frame shift (**Fig. 3a** and **Supplementary Fig. 3**). In PH-16900, all three siblings with microcephaly were homozygous for a missense p.Val65Met change (c.193G>A; **Fig. 3a** and **Supplementary Fig. 3**) that alters a residue conserved in all vertebrates (**Supplementary Fig. 4**). An unaffected sibling (PH-16907, with mild speech delay and articulation difficulties but with normal head circumference and normal MRI) was homozygous for the wild-type allele (**Supplementary Fig. 3**). Two additional unaffected siblings were homozygous and heterozygous, respectively, for the wild-type allele (not shown). None of these mutations were found in sequencing of 508 unaffected control individuals.

WDR62 encodes a 1,523 amino acid protein with multiple WD40 repeats (**Fig. 3a**)[6], but little is known about its function. A proteomic study identified WDR62 as a binding partner of the centrosomal protein CEP170[7], which is of interest given the involvement of other centrosomal proteins in microcephaly[8–14]. Another report

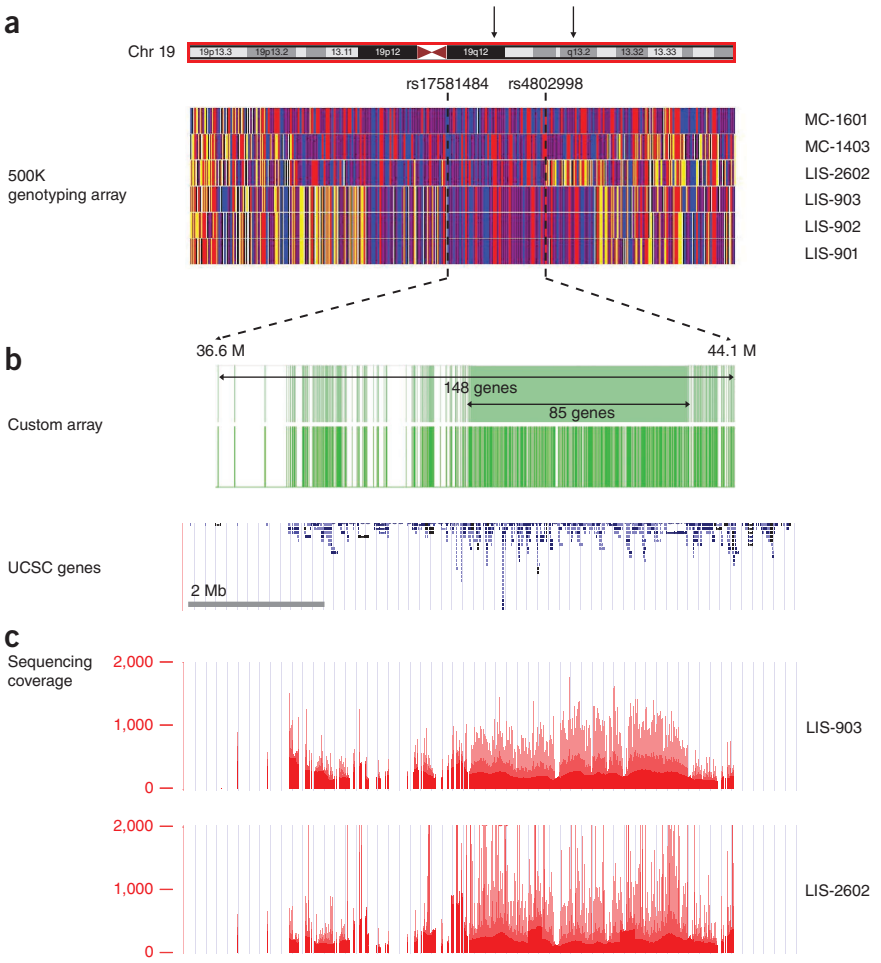

Figure 2 Mapping, capture and sequencing of 148 genes in the MCSG locus. (**a**) Homozygosity analysis in four pedigrees (LIS-900, LIS-2600, MC-1400 and MC-1600) revealed a 7.5-Mb interval on chromosome 19 bounded by SNP markers rs17581484 and rs4802998. Homozygous SNPs are shown in red or blue, heterozygous SNPs are shown in yellow and SNPs for which no genotype could be assigned are shown in white. The homozygous region contained 148 annotated UCSC genes. (**b**) Custom NimbleGen microarrays were designed to target all coding and noncoding regions of the 85 genes in the center of the linkage peak and all exonic regions of the remaining 63 genes (upper green track; the locations of probes on the array are shown on the lower track). These were used to capture genomic DNA and generate sequencing libraries from two individuals, LIS-903 and LIS-2602. (**c**) Libraries were sequenced on a Illumina GA II to an average read depth of >200 and a completeness of 88% to 90% (bases covered by ≥ 10 reads). The depth of sequence coverage over the region is shown.

identified WDR62 as a binding partner for c-Jun N-terminal kinase (JNK), suggesting that it potentiates JNK activity[15]. *In situ* hybridization with a probe to mouse *Wdr62* showed widespread expression in the developing brain at embryonic day (E) 14.5 (**Fig. 4a**), with the highest expression occurring in the forebrain. Expression was seen in the ventricular zone and the cortical plate (**Fig. 4b**), consistent with roles in progenitor cells and postmitotic neurons.

WDR62 demonstrates notable cell cycle–dependent localization. Immunofluorescence staining of endogenous WDR62 in HeLa cells with an anti-WDR62 antibody revealed punctate, perinuclear expression during interphase, suggesting localization to the Golgi apparatus, which was confirmed by GM130 immunoreactivity (**Fig. 4c**,**d**). In contrast, in HeLa or HEK cells in M phase, WDR62 is found at the spindle poles, as demonstrated by double labeling with γ-tubulin and dynein (**Fig. 4e**,**f**). Close inspection of recombinant HA-tagged WDR62 protein demonstrated subcellular localization closely matching that of CEP170 (**Fig. 4g**) and surrounding LIS1 (**Fig. 4h**), a pattern similar to that previously demonstrated for ASPM[16,17] and other microcephaly proteins[12,13,18,19]. A recent study[20] described mutations in *WDR62* associated with brain malformations and reported nuclear localization of WDR62 in cortical progenitor cells. Although we cannot rule out nuclear localization in some cells, our data, as well as previously published data[7] suggest a major centrosomal role.

Postmortem analysis of LIS-2601, an affected sibling in the LIS-2600 family[1], suggests roles for WDR62 in neuronal proliferation and migration. The 27-week fetus showed a small cranial cavity enclosing a profoundly small brain (weighing 50 g, compared to a normal weight of 127 g ± 20 g for this age and size fetus). The surface of the hemispheres was largely smooth (data not shown) with poorly defined Sylvian fissures and few sulci[1]. The cerebellum appeared remarkably preserved (data not shown), whereas the cerebral cortex was severely abnormal (**Fig. 5a**–**g**). The outermost cortical layer (layer I) appeared generally normal but the remaining cortical neuronal layers were thinner than normal (**Fig. 5b**,**c**). There was an almost complete lack of small- to medium-sized pyramidal neurons in their normal location (layers II and III), suggesting profoundly defective neurogenesis. Neurons located beneath layer I were primarily medium to large pyramidal neurons, followed by a cell-sparse zone and a third layer of multipolar neurons at the deepest layer of the cortex, an appearance consistent with layers V and VI, respectively (**Fig. 5c**,**d**). Neurons in the medium to large pyramidal layer retained an immature radial columnar organization and also exhibited abnormal, nonradial clumping (**Fig. 5d**). In some sections, the pial surface was interrupted by microscopic extrusions of cells into

Table 1 Variant filtering identifies *WDR62* as the causative gene for MCSG

	LIS-903	LIS-2602
Total variants	2,310	2,570
Rare variants not in dbSNP or 1000 Genomes Project	262	323
Pathogenic	93	99
Rare and pathogenic	5	7
Rare, pathogenic and in both families	*WDR62*	*WDR62*

Variant filtering identifies a single gene, *WDR62*, disrupted in two families with MCSG. Variants were filtered to remove common polymorphisms and then annotated to highlight variants with functional splicing or coding implications, reducing the number of candidate mutations in each individual to five in LIS-903 and seven in LIS-2602. Of these candidates, only one gene, *WDR62*, was disrupted in both families.

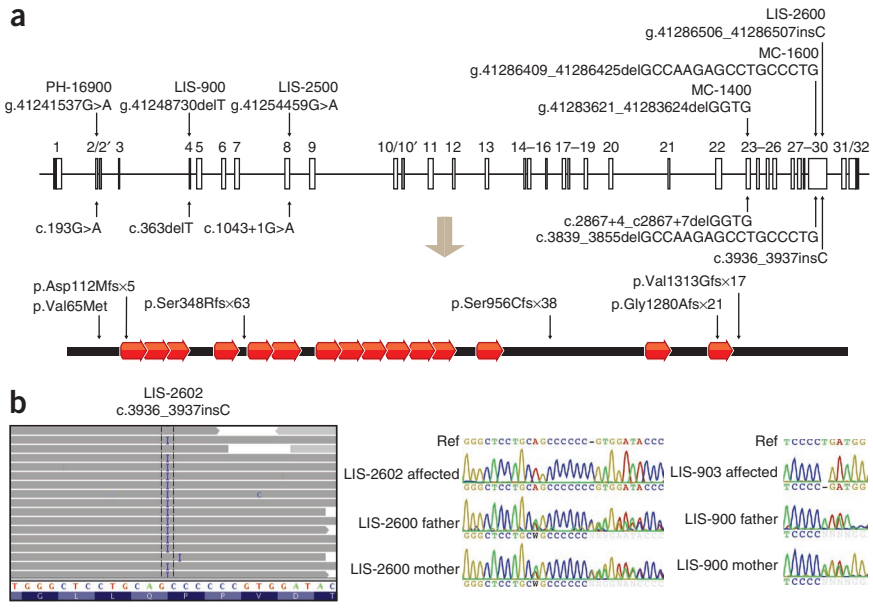

Figure 3 Six *WDR62* mutations reported in association with microcephaly with simplified gyri. (**a**) Alterations are shown in genomic, coding DNA and protein contexts. The human *WDR62* gene consists of 32 exons shown as boxes and encodes a protein of 1,518 amino acids containing 15 WD40 repeats. Black shaded boxes represent untranslated regions, open boxes represent coding regions, and gray shaded boxes represent alternatively spliced exons. Lines connecting the boxes represent introns. The diagram is drawn to scale. Five of the six alleles (from families LIS-900, LIS-2500, LIS-2600, MC-1400, MC-1600 and LIS-2600) disrupt splice sites or cause frame shifts resulting in protein truncations and are likely null alleles. The sixth allele, found in PH-16900, contains the missense alteration p.Val65Met and is a conserved residue (**Supplementary Fig. 4**). (**b**) Illustration of the c.3936_3937insC mutation in LIS-2602 by high throughput sequencing and representative Sanger traces confirming proper segregation. High throughput sequencing data is shown using the Integrated Genome Viewer. Aligned reads are shown as gray tags shaded by quality score, SNPs are identified by the letter code of the substituted base, and the position of the LIS-2602 single-basepair insertion is denoted by the letter I. Representative Sanger traces confirm this change in the affected individual and show that both parents are heterozygous for the insertional event. Similarly, representative Sanger traces illustrate the c.363delT mutation in LIS-903 and the carrier status of both parents.

the subarachnoid space, forming heterotopia (**Fig. 5e**). Heterotopia were also sometimes found in the intermediate zone, arranged in streaks, particularly in the posterior frontal cortex (**Fig. 5f**), corresponding to the localization of subcortical heterotopia seen on MRI. There were also clusters (**Fig. 5g**) of small round cells in the outer subventricular zone (SVZ) suggestive of progenitor cells. These findings support a proliferative defect in brains of individuals with *WDR62* mutations, potentially affecting the outer SVZ (precursors to upper layer cortical neurons)[21] as well as defective neuronal migration, in some ways evocative of the dual roles in proliferation and migration seen for *LIS1*[22,23].

Our results suggest that mutations in *WDR62* cause microcephaly, simplified gyral pattern, callosal abnormalities and a wide range of additional cortical abnormalities, including polymicrogyria, schizencephaly and subcortical heterotopia. *WDR62* lies within the *MCPH2* locus[24–26], a gene-rich locus that has resisted gene identification for >10 years and appears to be allelic to *MCPH2*. The remarkable diversity of cortical malformations associated with *WDR62* mutation suggests that it acts at a critical hub of human cerebral development.

URLs. 1000 Genomes Project, http://www.1000genomes.org/; UCSC Human Genome Browser, http://genome.ucsc.edu/; Human Splicing Finder Version 2.3, http://www.umd.be/HSF/.

METHODS

Methods and any associated references are available in the online version of the paper at http://www.nature.com/naturegenetics/.

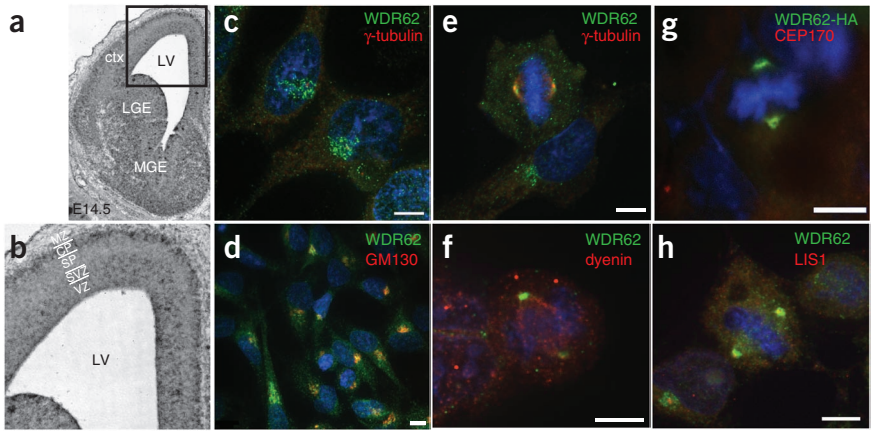

Figure 4 *WDR62* expression in developing mouse brain and subcellular localization. (**a**) *In situ* hybridization of E14.5 mouse brain with antisense probe to mouse *Wdr62*. Sense strand (data not shown) showed no specific hybridization. (**b**) Higher power view. A strong *WDR62* message is seen in the ventricular zone, subventricular zone, ventral portion of the intermediate zone and the ganglionic eminences, with some hybridization in the cortical plate. (**c**–**h**) Confocal microscopy demonstrating WDR62 subcellular localization. (**c**,**d**) Endogenous WDR62 localization in interphase HeLa cells. (**c**) Anti-WDR62 (green), also stained with anti γ-tubulin (red) and Hoechst for DNA (blue), showing perinuclear localization surrounding but not overlapping the centrosome. (**d**) Co-staining of interphase HeLa cells with anti-WDR62 and anti-GM130 shows localization of both to the Golgi apparatus near the Hoechst-positive nucleus. (**e**–**g**) WDR62 localization in HeLa and HEK cells during the M phase. (**e**) Endogenous WDR62 localizes to the spindle poles in M phase HeLa cells, visualized by double labeling with γ-tubulin. (**f**) Co-staining with antisera to WDR62 and dynein in HEK cells shows WDR62 at the spindle poles and dynein throughout the spindle. (**g**) Transfection of C-terminal HA-tagged WDR62 in HEK cells confirms ring-like localization around the centrosome and overlaps with CEP170, another centrosomal protein. (**h**) Endogenous WDR62 immunoreactivity surrounds LIS1 but does not overlap fully.

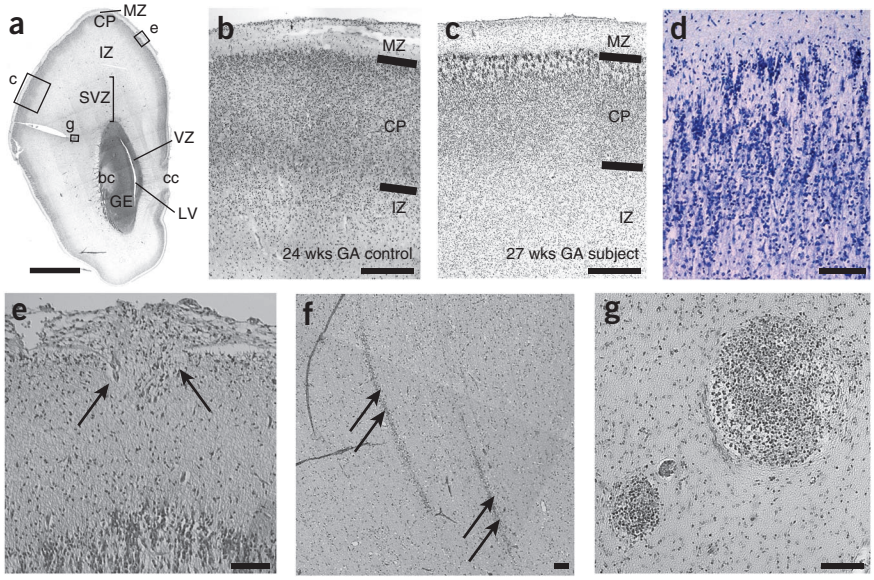

Figure 5 Histopathologic analysis of a 27-week-old human fetus with MCSG. (**a**) Hemotoxylin and eosin stained coronal section from the forebrain of a 27-week-old gestational age fetus with microcephaly with simplified gyri (LIS-2601). Section is at the rostral end of the caudate along the A-P axis. Locations of higher magnification views for panels **c**, **e** and **g** are indicated. (**b**,**c**) Hemotoxylin and eosin stained section demonstrating cortical layering. Compared to a 24-week gestational age control fetus (**b**), LIS-2601 has an abnormally thin cortical plate (despite being three weeks older; **c**), suggestive of a proliferative defect and an absence of normal-appearing layer II and III cells underneath the molecular layer. The dimensions of the marginal zone are relatively preserved. (**d**) In addition to a smaller cortical plate, neurons in the cortical plate display abnormal persistence of a radial columnar pattern and disorganized clustering, shown in a Kluver-Barrera stain. (**e**) Occasionally, eruptions of neuroglial cells (arrows) through the pial surface into the subarachnoid space are seen, as are occasional (**f**) streaky heterotopia in the intermediate zone and (**g**) clusters of small, darkly staining cells in the outer subventricular zone that resemble dividing cells. IZ, intermediate zone; GE, ganglionic eminence; LV, lateral ventricle; bc, body of the caudate; cc, corpus callosum; ctx, cortex; LGE, lateral ganglionic eminence; MGE, medial ganglionic eminence; MZ, marginal zone; CP, cortical plate; SP, subplate; SVZ, subventricular zone; VZ, ventricular zone.

Accession codes. Human *WDR62* mRNA: RefSeq NM_001083961.1; Human WDR62 Protein: RefSeq NP_001077430; Mouse *Wdr62* mRNA: IMAGE clone 6405269, GenBank accession BC054747.

Note: Supplementary information is available on the Nature Genetics website.

ACKNOWLEDGMENTS

We thank the many families and researchers who participated in this study; B. Chang and A. Poduri for expert review of MRI imaging findings; S. Lizarraga for contributions to genetic mapping; M. Aita and the *In situ* Hybridization Core Facility, University of North Carolina Neuroscience Center, Chapel Hill, North Carolina for performing *in situ* hybridizations; C.G. Woods for helpful discussions and for sharing data before publication; A. von Deimling from the Institut für Pathologie, Heidelberg, for sectioning of the LIS-2601 brain; A. Nicholas and M. Khurshid for advice regarding immunohistochemistry; A. Hill and L. Bu at the MRDDRC (Mental Retardation Developmental Disability Research Center) Imaging Core for assistance with confocal microscopy (US National Institutes of Health (NIH) grant P30-HD-18655 and Fidelity Foundation); and R. Sean Hill for assistance with linkage analysis and helpful discussions. We are indebted to the members of the Microcephaly Collaborative (**Supplementary Table 1**) for contributing to the cohort from which these families were drawn. T.W.Y. was supported by a NIH T32 grant (T32 NS007484-08), the Clinical Investigator Training Program (CITP) at Harvard-Massachusetts Institute of Technology Health Sciences and Technology and Beth Israel Deaconess Medical Center in collaboration with Pfizer, Inc. and Merck and Company, Inc., and the Nancy Lurie Marks Junior Faculty MeRIT Fellowship. G.H.M. was supported by the Young Investigator Award of National Alliance for Research on Schizophrenia and Depression (NARSAD) as a NARSAD Lieber Investigator. Research was supported by grants from the National Institute of Neurological Disorders and Stroke (NINDS) (RO1 NSR01-35129) and the Fogarty International Center (R21 NS061772) to C.A.W., the Dubai Harvard Foundation for Medical Research and the Manton Center for Orphan Disease Research. Genotyping services were provided by the Center for Inherited Disease Research (CIDR). CIDR is funded through a federal contract from the NIH to Johns Hopkins University, contract number HHSN268200782096C and NIH N01-HG-65403. Genotyping at Children's Hospital Boston was supported by the Intellectual and Developmental Disabilities Research Centers (CHB DDRC, P30 HD18655). Genotyping at the Broad Institute was supported by National Human Genome Research Institute (NHGRI). C.A.W. is an investigator of the Howard Hughes Medical Institute.

AUTHOR CONTRIBUTIONS

T.W.Y. helped characterize MCSG syndrome, designed and performed targeted capture experiments, generated sequencing libraries, designed bioinformatics pipelines, analyzed sequencing data, identified *WDR62* mutations, designed *WDR62 in situ* expression studies, designed, performed and analyzed WDR62 immunohistochemistry studies, helped analyze the LIS-2601 postmortem specimen and wrote the manuscript. G.H.M. helped characterize MCSG syndrome, performed initial genome wide linkage studies and identified the MCSG locus. D.J.T. designed and performed WDR62 immunohistochemistry studies, helped analyze *in situ* expression studies and helped analyze the LIS-2601 postmortem specimen. S.K.S. helped characterize MCSG syndrome, identified additional affected families, analyzed SNP and microsatellite genotyping and narrowed the MCSG genomic interval. L.F.-S. helped characterize MCSG syndrome and wrote the initial clinical description of the LIS-900 family. C.M.S. identified the LIS-2600 family and provided clinical information and the LIS-2601 postmortem specimen. M.T. identified the MC-1400 and MC-1600 families and provided clinical information. M.T.M. identified the PH-16900 family and provided clinical information. B.J.B. organized clinical information and subject samples. J.M.F. sequenced *WDR62* in families to confirm high throughput sequencing findings and to discover additional alleles. C.S. helped with bioinformatic pipelines and generated constructs for *WDR62 in situ* expression studies. W.B.D. referred the PH-16900 family. R.D.F. analyzed the LIS-2601 postmortem specimen. A.J.B. reviewed MRIs for characterization of MCSG syndrome. C.A.W. directed the overall research, helped analyze the LIS-2601 postmortem specimen and wrote the manuscript.

COMPETING FINANCIAL INTERESTS

The authors declare no competing financial interests.

Published online at http://www.nature.com/naturegenetics/.
Reprints and permissions information is available online at http://npg.nature.com/reprintsandpermissions/.

1. Sergi, C., Zoubaa, S. & Schiesser, M. Norman-Roberts syndrome: prenatal diagnosis and autopsy findings. *Prenat. Diagn.* **20**, 505–509 (2000).
2. Albert, T.J. *et al.* Direct selection of human genomic loci by microarray hybridization. *Nat. Methods* **4**, 903–905 (2007).
3. Li, H. & Durbin, R. Fast and accurate short read alignment with Burrows-Wheeler transform. *Bioinformatics* **26**, 589–595 (2009).
4. Sherry, S.T. *et al.* dbSNP: the NCBI database of genetic variation. *Nucleic Acids Res.* **29**, 308–311 (2001).
5. Desmet, F.-O. *et al.* Human Splicing Finder: an online bioinformatics tool to predict splicing signals. *Nucleic Acids Res.* **37**, e67 (2009).
6. Li, D. & Roberts, R. WD-repeat proteins: structure characteristics, biological function, and their involvement in human diseases. *Cell. Mol. Life Sci.* **58**, 2085–2097 (2001).
7. Hutchins, J.R.A. *et al.* Systematic analysis of human protein complexes identifies chromosome segregation proteins. *Science* **328**, 593–599 (2010).

8. Bond, J. & Woods, C.G. Cytoskeletal genes regulating brain size. *Curr. Opin. Cell Biol.* **18**, 95–101 (2006).
9. Rauch, A. *et al.* Mutations in the pericentrin (*PCNT*) gene cause primordial dwarfism. *Science* **319**, 816–819 (2008).
10. Bond, J. *et al.* A centrosomal mechanism involving CDK5RAP2 and CENPJ controls brain size. *Nat. Genet.* **37**, 353–355 (2005).
11. Feng, Y. & Walsh, C.A. Mitotic spindle regulation by Nde1 controls cerebral cortical size. *Neuron* **44**, 279–293 (2004).
12. Lizarraga, S.B. *et al.* Cdk5rap2 regulates centrosome function and chromosome segregation in neuronal progenitors. *Development* **137**, 1907–1917 (2010).
13. Kouprina, N. *et al.* The microcephaly *ASPM* gene is expressed in proliferating tissues and encodes for a mitotic spindle protein. *Hum. Mol. Genet.* **14**, 2155–2165 (2005).
14. Thornton, G.K. & Woods, C.G. Primary microcephaly: do all roads lead to Rome? *Trends Genet.* **25**, 501–510 (2009).
15. Wasserman, T. *et al.* A novel c-Jun N-terminal kinase (JNK)-binding protein WDR62 is recruited to stress granules and mediates a nonclassical JNK activation. *Mol. Biol. Cell* **21**, 117–130 (2010).
16. Saunders, R.D., Avides, M.C., Howard, T., Gonzalez, C. & Glover, D.M. The *Drosophila* gene abnormal spindle encodes a novel microtubule-associated protein that associates with the polar regions of the mitotic spindle. *J. Cell Biol.* **137**, 881–890 (1997).
17. van der Voet, M. *et al.* NuMA-related LIN-5, ASPM-1, calmodulin and dynein promote meiotic spindle rotation independently of cortical LIN-5/GPR/G-α. *Nat. Cell Biol.* **11**, 269–277 (2009).
18. Faulkner, N.E. *et al.* A role for the lissencephaly gene *LIS1* in mitosis and cytoplasmic dynein function. *Nat. Cell Biol.* **2**, 784–791 (2000).
19. Bond, J. *et al.* ASPM is a major determinant of cerebral cortical size. *Nat. Genet.* **32**, 316–320 (2002).
20. Bilguvar, K. *et al.* Whole-exome sequencing identifies recessive *WDR62* mutations in severe brain malformations. *Nature* **467**, 207–210 (2010).
21. Hansen, D.V., Lui, J.H., Parker, P.R.L. & Kriegstein, A.R. Neurogenic radial glia in the outer subventricular zone of human neocortex. *Nature* **464**, 554–561 (2010).
22. Gambello, M.J. *et al.* Multiple dose-dependent effects of Lis1 on cerebral cortical development. *J. Neurosci.* **23**, 1719–1729 (2003).
23. Sheen, V.L. *et al.* Impaired proliferation and migration in human Miller-Dieker neural precursors. *Ann. Neurol.* **60**, 137–144 (2006).
24. Roberts, E. *et al.* Autosomal recessive primary microcephaly: an analysis of locus heterogeneity and phenotypic variation. *J. Med. Genet.* **39**, 718–721 (2002).
25. Gul, A. *et al.* Genetic studies of autosomal recessive primary microcephaly in 33 Pakistani families: novel sequence variants in *ASPM* gene. *Neurogenetics* **7**, 105–110 (2006).
26. Roberts, E. *et al.* The second locus for autosomal recessive primary microcephaly (MCPH2) maps to chromosome 19q13.1–13.2. *Eur. J. Hum. Genet.* **7**, 815–820 (1999).

ONLINE METHODS

Human studies. All human studies were reviewed and approved by the institutional review board of the Children's Hospital, Boston, the Beth Israel Deaconess Medical Center and the local institutions.

Genome-wide linkage scans. Family LIS-900 underwent a microsatellite genome-wide linkage screen at the Center for Inherited Disease Research (CIDR) using ~400 markers with a 10 cM average density. Genome-wide screens for Family LIS-2600 were performed at Children's Hospital Boston using ~400 markers in the ABI linkage mapping set MD v2.5 at a ~10 cM average density (Applied Biosystems). In addition, families LIS-900, LIS-2600, LIS-2500, MC-1400 and MC-1600 were genotyped on Affymetrix 5.0 SNP chips at the Broad Institute.

Fine mapping was done using polymorphic microsatellite markers from the ABI linkage mapping set HD v2.5 at a 5 cM average density (Applied Biosystems) and additional microsatellite markers identified using the UCSC Human Genome Browser. Singlepoint and multipoint LOD scores were calculated using Allegro, assuming a recessive mode of disease inheritance, full penetrance and a disease allele frequency of 0.0001. Nucleotide numbers are provided in reference to genomic coordinates (human genome build hg18), coding DNA coordinates (based on RefSeq mRNA NM_001083961.1, where A of the ATG translational start site is designated bp 1 and positioning within an intron are designated relative to the most 3 base of the nearest upstream coding exon), or protein coordinates (based UniProt accession number O43379), following HGVS guidelines[27].

Microarray sequence capture and sequencing. After flanking recombinant markers were used to define the candidate interval, a tiled microarray (Roche NimbleGen) was designed to target all exons of the 148 genes in the region, as well as most of the nonrepetitive intronic DNA for the 85 genes in the center of the linkage peak. A total of 3.5 Mb of the ~7.5-Mb region was targeted. From each affected individual, 20 µg of genomic DNA was randomly fragmented to 350–400 bp and the ends were repaired and ligated to NimbleGen gSel adaptors. This library was hybridized to the custom array using the manufacturer's recommended conditions, and nonbound DNA was washed off. Bound DNA was eluted and subjected to PCR amplification. qPCR showed ×355 target enrichment for LIS-903 and ×1,346 enrichment for LIS-2601. Nimblegen-captured DNA fragments were then blunted using T4 DNA Polymerase and Klenow fragment using standard conditions, phosphorylated using T4 DNA kinase and ligated to form concatamers. The concatamers were then randomly fragmented using a Covaris S2 device, and the ends were repaired and ligated to Illumina-paired end sequencing adaptors. Ligated products were gel purified and PCR amplified to enrich for adaptor-containing fragments. Finally, the purified DNA was subjected to clustering and 40 cycles of paired-end sequencing using the Illumina GA II. Sequencing and subsequent image processing and base calling were performed per the manufacturer's recommended conditions.

DNA sequence analysis. High-throughput sequence analysis was performed according to a customized bioinformatic pipeline for tracking sequence data, aligning reads, calculating coverage, calling variants, annotating variants with respect to functional effect, filtering out benign variation and flagging candidate rare, pathogenic mutations. Briefly, BWA version 0.5.7 (ref. 3) was employed to align short reads to the human genome (reference build hg18). Consensus and variant base calls were made with SAMtools version 0.1.7, filtered for quality and mapping confidence, and loaded into a MySQL database for storage and further processing, including annotation of the predicted consequences (noncoding, coding synonymous, coding nonsynonymous or frameshift, splice site) of each variant using GMCC[28]. Candidate mutations were identified by starting with a list of all variants from the targeted homozygous region, removing those present either in dbSNP130 or a pilot 1 release of the 1000 Genomes Project database and selecting for coding nonsynonymous, frameshift or splice site changes. Sequence data were visualized using either the UCSC Genome Browser[29] or the Broad Institute Integrated Genome Viewer. All genomic base positions are presented in reference to the human genome NCBI build 36 (hg18).

Sequencing of WDR62 in controls. Coding WDR62 exons and at least 50 base-pairs of flanking sequence were PCR amplified and submitted for Sanger capillary electrophoresis (Polymorphic DNA Technologies) in accordance with standard methods. Samples included 384 neurologically normal control samples (Coriell) and 124 unaffected individuals from Middle Eastern families with unrelated disorders.

Evidence for four unvalidated *WDR62* variants deposited in dbSNP was also reviewed; rs34840924, rs35055110, rs35938064 and rs34734597 are single basepair insertions in *WDR62* coding regions that would be predicted to cause frameshifts but which were unvalidated SNPs ascertained from a single study of five individuals (Submitted batch ID xplore_hum_chr19_2, Submitter Population ID Celera_Donors). Sequencing in 508 controls failed to confirm the existence of these variants.

*Probe preparation***.** Plasmid templates for riboprobe synthesis were generated by restriction digestion of mouse Wdr62 IMAGE cDNA clone 6405269 to contain a 574-bp sequence corresponding to nucleotide position 4,227–4,801 of the cDNA. Digoxigenin-labeled sense and antisense RNA probes were synthesized using the DIG RNA Labeling kit (Roche Molecular Biochemicals).

In situ hybridization. In situ hybridization was performed as described[30]. Sections were hybridized at 65 °C for 12–16 h in 1–2 µg/ml of riboprobe and then washed. After blocking for 1 h at room temperature (20–25 °C), sections were labeled with anti-DIG Fab-AP antibody (1:2000 dilution; Roche) for 2 h at room temperature and then washed and developed in NBT (nitroblue-tetrazolium-chloride) with BCIP (5-bromo-4-chloro-indolyl-phosphate) at room temperature until ideal intensity was reached.

Immunocytochemistry. HeLa cells were fixed with ice-cold methanol and placed at −20 °C for 5 min. The cells were blocked in ×1 TBS with 0.15% Tween containing 5% normal donkey serum (vol/vol) for one hour at room temperature. Cells were then incubated for 3 h at room temperature in primary antibody diluted in blocking solution. For primary antibodies, we used mouse monoclonal anti γ-tubulin (Abcam, ab27074, 1:2000), rabbit polyclonal anti-WDR62 (Bethyl laboratories, A301-560A, 1:500), mouse monoclonal anti-GM130 (BD Transduction Laboratories, 610822), mouse monoclonal anti-dynein heavy chain (Abcam, ab6305, 1:50), rat monoclonal anti-HA (Roche, 3F10, 1:500), rabbit anti-CEP170 (Abcam, ab72505, 1:100) and rabbit polyclonal anti-LIS1 (Bethyl laboratories, A300-409A, 1:200). Cells were then washed three times with PBS and incubated with secondary antibodies against the appropriate species (DyLight, Jackson Labs, 1:200) in blocking solution for 1 h at room temperature. The cells were then washed twice with blocking solution and incubated with Hoechst 33342 (1:2000, Invitrogen) for 5 min at room temperature. Cells were then washed twice with ×1 PBS, mounted with Fluoromount-GT and left at 4 °C overnight to dry. For ICC requiring the use of primary antibodies raised in the same host species, cells were fixed and blocked according to standard procedures and then incubated with the first primary antibody for 3 h. Cells were then washed three times with blocking solution and incubated with Cy3-conjugated Fab fragments of anti-rabbit IgG (Jackson ImmunoResearch Laboratories) for secondary detection. Cells were then washed four times with blocking solution and incubated with unconjugated Fab fragments of anti-rabbit IgG for two hours. After washing the cells four times with blocking solution, the second primary antibody was applied and detected using the previously described protocol.

Recombinant HA-WDR62. A full-length human WDR62 cDNA (IMAGE Consortium clone 4510905) was obtained and used for site-directed mutagenesis (Quikchange, Agilent) to introduce the HA epitope immediately upstream of the stop codon. WDR62-HA was cloned downstream of the CMV promoter, transfected into HEK cells with lipofectamine and processed for immunocytochemistry at 24 h.

27. den Dunnen, J.T. & Antonarakis, S.E. Mutation nomenclature extensions and suggestions to describe complex mutations: a discussion. *Hum. Mutat.* **15**, 7–12 (2000).
28. Major, J.E. Genomic mutation consequence calculator. *Bioinformatics* **23**, 3091–3092 (2007).
29. Kent, W.J. *et al.* The Human Genome Browser at UCSC. *Genome Res.* **12**, 996–1006 (2002).
30. Tucker, E.S. *et al.* Molecular specification and patterning of progenitor cells in the lateral and medial ganglionic eminences. *J. Neurosci.* **28**, 9504–9518 (2008).